J Solid State Electrochem (2009) 13:1905–1911
DOI 10.1007/s10008-008-0752-7

ORIGINAL PAPER

Dip-coating and co-sintering technologies for fabricating tubular solid oxide fuel cells

R. Z. Liu · S. R. Wang · Bo Huang · C. H. Zhao · J. L. Li · Z. R. Wang · Z. Y. Wen · T. L. Wen

Received: 29 October 2008 / Revised: 13 November 2008 / Accepted: 20 November 2008 / Published online: 20 December 2008

Abstract A dip-coating method to fabricate anode-supported tubular solid oxide fuel cells has been successfully developed. The length, outside diameter, and thickness of the single cell are 10.8 cm, 1.0 cm, and 0.6 mm, respectively. The area of the cathode is 15–16 cm^2 (cathode length=4.8 cm). The cell consists of a Ni-YSZ anode support tube, a Ni-ScSZ anode functional layer, a ScSZ electrolyte film, a LSM-ScSZ cathode functional layer, and a LSM cathode current collecting layer. A preliminary examination of the single tubular cell has been carried out and an acceptable performance was obtained. The maximum power density was, respectively, 325, 276, 208, and 168 mW cm^{-2} at 850, 800, 750, and 700 °C, when operating with humidified hydrogen.

Keywords Solid oxide fuel cell (SOFC) · Tubular · Anode-supported · Dip-coating method · Fabrication

Introduction

Solid oxide fuel cells (SOFCs) are solid device that convert the chemical energy of fuels to electricity by electrochemical oxidation. They have a high thermodynamic efficiency and can operate on many different fuels [1]. The traditional high temperature SOFCs, which is based on an electrolyte support and operated at 1,000 °C, have many problems, such as limited materials selection, high materials cost, etc [2]. Thus, reduced temperature SOFCs are being extensively studied because of the technical and economic benefits of reducing the operating temperature down to 600–800 °C. The cost of SOFC technology can be dramatically reduced since much less expensive materials can be used in cell construction, and novel fabrication techniques can be applied to the stack and system integration. Further, as the operating temperature is reduced, so the possibility of using SOFCs for a wide variety of applications, including residential and automotive applications, increase as does system reliability and operational life increase [3–9]. Using an anode support allows a thin-coated electrolyte to be placed on the supporting anode, which reduces electrolytic resistance losses and yields better conductance at lower temperatures [10–12] over an electrolyte support.

There are two main types of design for SOFCs: planar and tubular. Tubular SOFCs have many advantages [13–16] such as ease in sealing and the ability to endure the thermal stress caused by rapid heating up to operating temperature. Kendall and Palin [14] and Yashiro et al. [15] have reported that small-scale tubular SOFCs can endure the thermal stress caused by rapid heating up to the operating temperature. Tubular SOFCs can therefore be expected to be used for co-generation and transportation applications.

Fabrication is one of the major focuses of cost reduction. Many methods for fabricating tubular SOFCs have been well documented in recent years: extrusion [1, 17, 18], plasma spraying [19, 20], gelcasting [2], etc. But, they have a number of shortcomings, such as high investment in large equipment, complicated fabrication processes, and long production cycle. In our previous work, we have reported a simple dip-coating method to prepare anode-supported tubular SOFCs [21]. It has many advantages over conventional forming process, such as isostatic pressing, extrusion, plasma spraying, gelcasting, etc. First of all, it neither needs

R. Z. Liu (✉) · S. R. Wang · B. Huang · C. H. Zhao · J. L. Li · Z. R. Wang · Z. Y. Wen · T. L. Wen
Shanghai Institute of Ceramics,
Chinese Academy of Sciences (SICCAS),
1295 Dingxi Road,
Shanghai 200050, People's Republic of China
e-mail: lrzox@mail.sic.ac.cn

large equipment nor needs controlling the ambience severely; so, the fabrication cost is very low. Secondly, it was a simple fabrication process; it just only repeats the dip-coating actions with sintering. Thirdly, it can be applied both in laboratory and industry scale by reason of the foregoing advantages. The purpose of this study was to improve and perfect the earlier work. In the cells fabrication process, we used the co-sintering technology to reduce the sintering times, with a view farther to reduce the fabrication cost and to simplify the fabrication process. In the size of cells side, large-scale tubular SOFCs, which are more suitable for application, have been fabricated successfully. In the structure of cell side, we used $(La_{0.8}Sr_{0.2})_{0.98}MnO_3$ (LSM, lanthanum strontium manganite, Inframet Advanced Materials, CT, USA) composite cathode material to improve the stability of the cell. To overcome the poor activity of the LSM cathode, on the one hand, we used $Zr_{0.89}Sc_{0.1}Ce_{0.01}O_{2-x}$ (ScSZ, scandia-stabilized zirconia, Daiichi Kigenso Kagaku Kogyo, Japan) substituting $Zr_{0.92}Y_{0.08}O_{2-x}$ (YSZ, yttria-stabilized zirconia, 99.99% pure, TOSO, Japan) as the electrolyte to increase the activity of the three-phase boundary of electrolyte/cathode; on the other hand, pure LSM was used as the cathode current collecting layer material. At the same time, the anode functional layer was changed to NiO-ScSZ. Consequently, we obtained a NiO-YSZ/NiO-ScSZ/ScSZ/LSM-ScSZ/LSM structure for the tubular SOFC.

Experimental

Fabrication of tubular SOFC

Figure 1 represents the fabrication process for the tubular cell by dip-coating method. Before dip coating, the slurries of all the components were prepared by ball-milling method. For example, the anode support tube slurry, which contains commercial nickel oxide (NiO, Inco, Canada) powder and YSZ powder (50% NiO and 50% YSZ by mass; Fuel Cell Materials) was first prepared. An azeotropic mixture of butanone and ethyl alcohol was used as the solvent, triethanolamine as a kind of zwitterionic dispersant to reduce the tension in the interface between the surface of the particle and the liquid, polyethylene glycol (PEG 200)

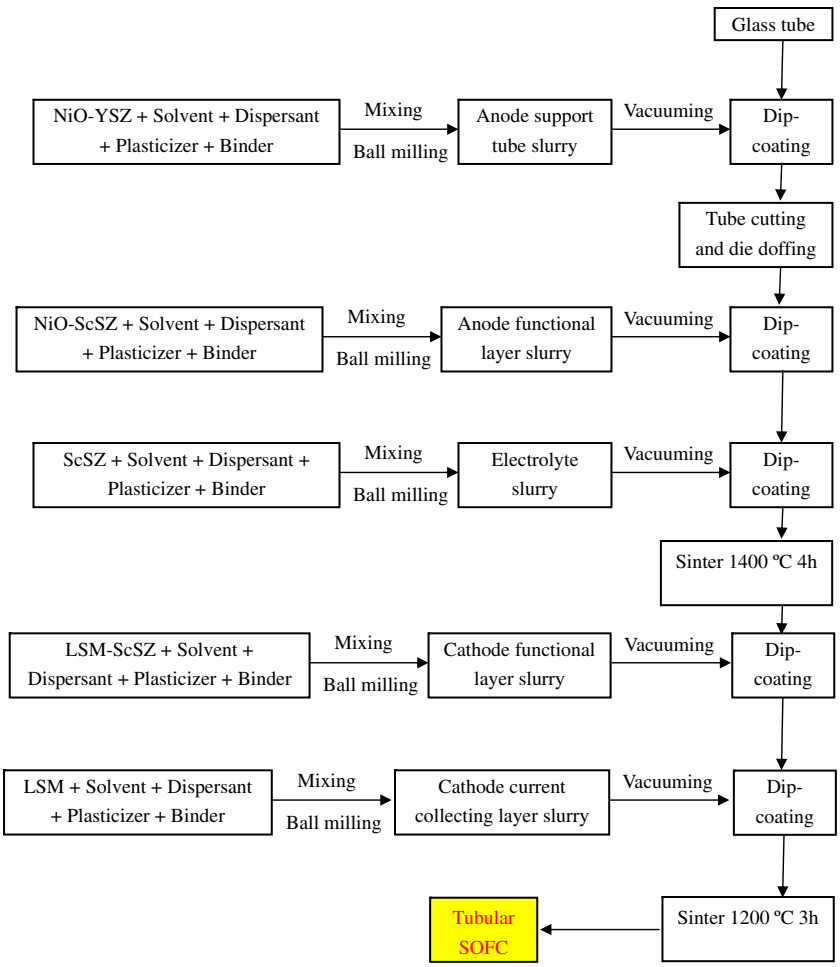

Fig. 1 Fabrication process of the anode-supported tubular single cell

as a plasticizer to increase the flexibility of the tube, and poly-vinyl-butyl as the binder to provide sufficient strength after the solvent had evaporated. All the organic additives were supplied by Shanghai Chem., China. The starting materials were weighed, mixed, and ball-milled. Homogeneous slurry was then obtained. It was degassed using a vacuum pump (pressure, 200 mbar absolute). Other slurries were prepared in the same way but with different quantity of organic additives. The dip-coating process was then carried out using a glass tube that was closed at one end. The glass tube was dipped in the slurry for 10 s then slowly drawn up. This dip-coating action was repeated several times to obtain the desired thickness. The green tube was then allowed to dry at room temperature for 48 h. When the solvent had completely evaporated, the anode-supported NiO-YSZ tube was moved from the glass tube and cut to the required length. The green NiO-YSZ tube was then dip-coated in NiO-ScSZ slurry and ScSZ slurry to prepare the anode functional layer and electrolyte membrane. After drying, the green tube was co-sintered at 1,400 °C for 4 h in air and then checked for gas tightness of the electrolyte by red ink. The red ink was dropped on the tube to cover the surface of the electrolyte. Then, the tube was put into the running water after 10 min to see if the red ink trace was left or not. If there was no red ink trace, it indicated that the electrolyte was dense enough.

The anode tube with dense electrolyte was then dip-coated in the LSM-ScSZ cathode functional layer slurry and the LSM cathode current collecting layer slurry, ordinally. At the same time, the reference cathode was dip-coated on the bottom of the tube. The cathode was dried and sintered at 1,200 °C for 3 h in air to complete a cell. The anode-supported tubular cell (length approx. 10.8 cm, outside diameter approx. 1.0 cm, thickness approx. 0.5–0.6 mm) was then obtained.

Cell performance test

The porosity of the anode support tube sintered at 1,400 °C was measured before and after reduction using a method based on Archimedes' principle by measuring the mass of water that could be absorbed into the porous tube (Archimedes' drainage).

SOFC tests were carried out in a single-cell test setup, shown in Fig. 2. A Pt mesh and Pt lead wires were attached to the surface of the cathode using Pt paste. On the anode side, a Ni foam and Pt lead wire (the thermoelectricity potential engendered between the two different metals can be ignored) were used as the current collector and were attached using Pt paste. An alumina tube was put inside the tubular single cell and used to lead the fuel gas. Humidified hydrogen was used as fuel and oxygen was used as oxidant. The fuel and oxidant flow rate were controlled at 200 and 120 smL min^{-1}, respectively. The current–voltage (*I–V*) curves and electrochemical impedance spectroscopies (EIS) were obtained to evaluate the performance of the cell. The *I–V* curves were obtained by the volt–ampere method. The EIS were obtained using an Electrochemical Workstation IM6ex (Zahner, GmbH, Germany). These measurements were started once the system had been adequately stabilized under a constant current of 2 A for 1 h. The current was then switched off, and the impedance spectra of the electrochemical cell were recorded under open circuit and under constant current densities of 66.7 and 133 mW cm^{-2}, with amplitude of 20 mV over the frequency range 0.03 Hz to 1 MHz. At the same time, the EIS of the anode to reference cathode and the cathode to reference cathode were measured under open circuit. The measurements were carried out at 700–850 °C, in steps of 50 °C. The ohmic resistances (R_Ω) were estimated from the high-frequency intercepts with the real axis, and the overall electrode

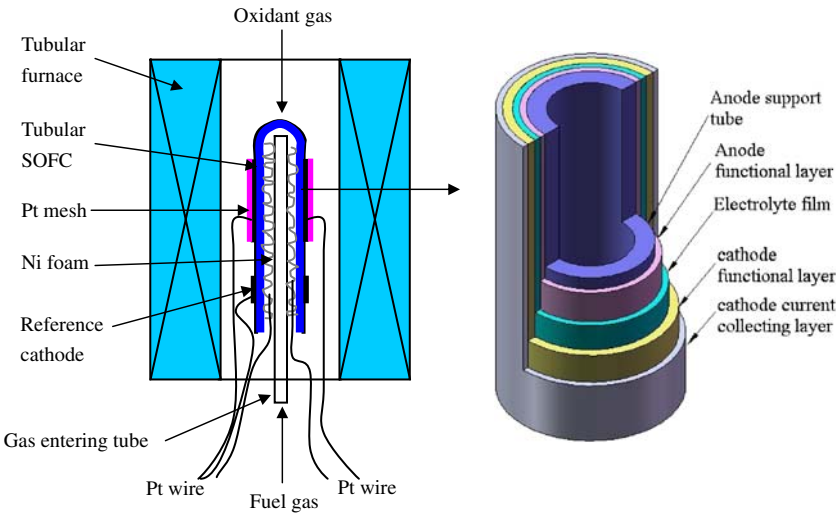

Fig. 2 Testing setup for the tubular single cell measurement and the structure of cell

polarization resistances (R_E) were directly measured from the differences between the low- and high-frequency intercepts with the real axis.

In order to observe the microstructure of the electrodes and the electrolyte, scanning electron microscope (SEM) images were observed with an electron probe microanalyzer (JXA-8100, JEOL) for the cross-section before and after the cell operation.

Results and discussion

Structure characteristics of anode-supported tubular SOFC

Figure 3 shows a NiO-YSZ anode-supported tubular single cell with reference cathode. The length of the cell was 10.8 cm (cathode length=4.8 cm), the outside diameter of the tube was 1.0 cm, the thickness of the tube was 0.5–0.6 mm, and the area of the cathode reached 15–16 cm^2. Figure 4 shows cross-sectional SEM micrographs of the tubular SOFC after testing. We found that the thickness of the electrolyte, the anode functional layer, the cathode functional layer, and the cathode current collecting layer were about 10, 5, 40, and 30 μm, respectively. The anode and cathode were porous with fine grains. The interfaces between anode/electrolyte and electrolyte/cathode were both good.

The microstructure of the anode support tube before and after reduction is shown in Fig. 5a and b. The micrographs indicate that the anode support tubes are porous before and after reduction. The porosity of the tube increases after reduction due to the NiO is deoxidized. The porosities of the support anode tube sintered at 1,400 °C were 21.95% and 34.83%, respectively, before and after reduction. In Fig. 5b, the larger grains are Ni particles and the smaller grains are YSZ particles, and the distribution of Ni particles, YSZ grains, and micropores is homogeneous.

Fig. 3 An anode-supported tubular SOFC with the length of 10.8 cm

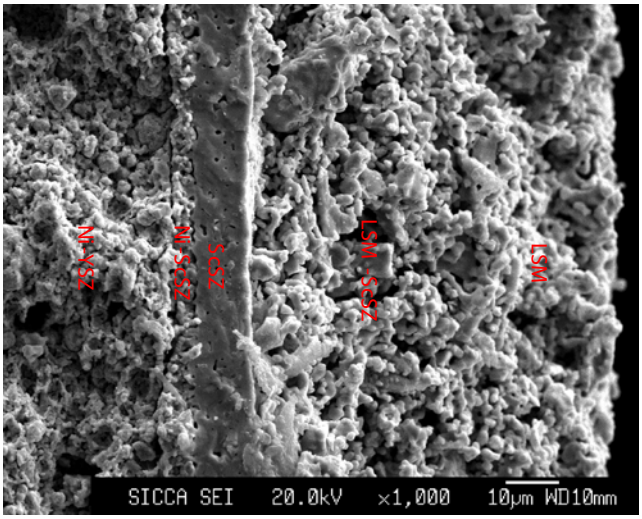

Fig. 4 Cross-section SEM image of the Ni-YSZ/Ni-ScSZ/ScSZ/LSM-ScSZ/LSM SOFC after testing

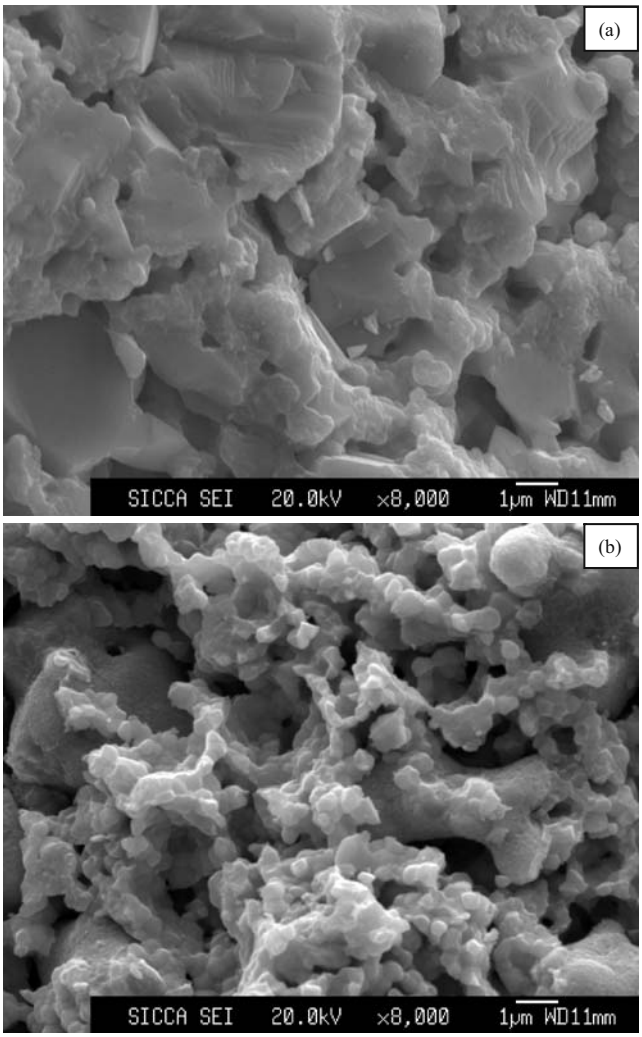

Fig. 5 SEM image of the Ni-YSZ anode support tube **a** before and **b** after testing

Good distribution of the Ni particles in the anode increases the number of electrode reaction sites by increasing the triple-phase boundary and current path [22].

Figures 6 and 7 show, respectively, the SEM micrograph of the LSM-ScSZ cathode functional layer and the LSM cathode current collecting layer after fuel cell testing. The cathode has a porous structure, and the grains were distributed over two scales in the cathode functional layer. The larger grains with an average grain size of approx. 2–3 μm were ScSZ grains, which can conduct oxygen ions. The smaller grains with an average grain size of approx. 0.5–1 μm were LSM grains, which were electron conductors. The micropores, ScSZ grains, and the LSM grains constitute a three-phase boundary. The LSM grains in the cathode current collecting layer were larger than those in the cathode functional layer; this can increase the pore size and improve the diffusivity of the oxygen [23].

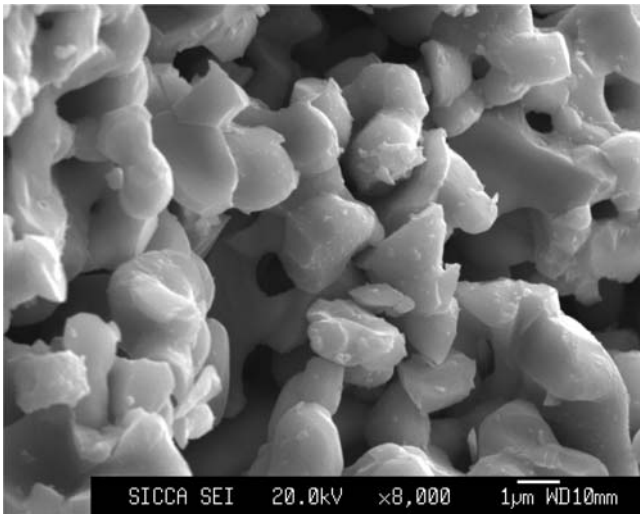

Fig. 7 SEM image of the LSM cathode current collecting layer after testing

Electrochemical performance of anode-supported tubular SOFC

Figure 8 shows the typical potential and power density versus the current density curves for the anode-supported tubular SOFC while running on humidified hydrogen at different temperatures. It can be seen that the open-circuit voltages (OCV) were 1.10–1.13 V in the temperature range; this was close to the theoretical values. It reveals that the electrolyte was dense enough to give higher values for the OCV. The performance of the cell was acceptable with a maximum power density of 325, 276, 208, and 168 mW cm^{-2} at 850, 800, 750, and 700 °C, respectively.

The AC impedance spectra for the anode-supported tubular cell at different temperatures using humidified hydrogen as fuel and oxygen as oxidant under open circuit are shown in Fig. 9. The ohmic resistances (R_Ω) and the electrode polarization resistances (R_E) increased as the temperature decreased. The ohmic resistances (R_Ω) were 0.72, 0.96, 1.03, and 1.14 Ω cm^2 at 850, 800, 750, and 700 °C, while the electrode polarization resistances (R_E) were 0.80, 1.12, 1.62, and 2.35 Ω cm^2, respectively. Figure 10 shows the AC impedance spectra for the cell under different current densities at 850 °C. The ohmic resistances (R_Ω) were constant under different current densities, but the electrode polarization resistances (R_E) decreased as the current densities increased. The electrode polarization resistances (R_E) were 0.80, 0.55, and 0.38 Ω cm^2, under

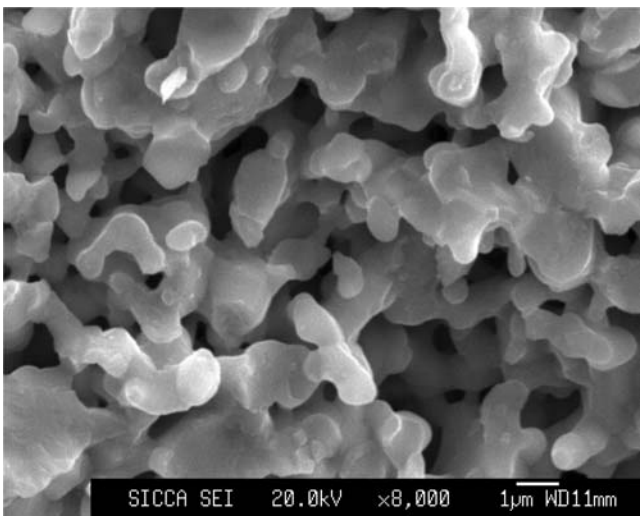

Fig. 6 SEM image of the LSM-ScSZ cathode functional layer after testing

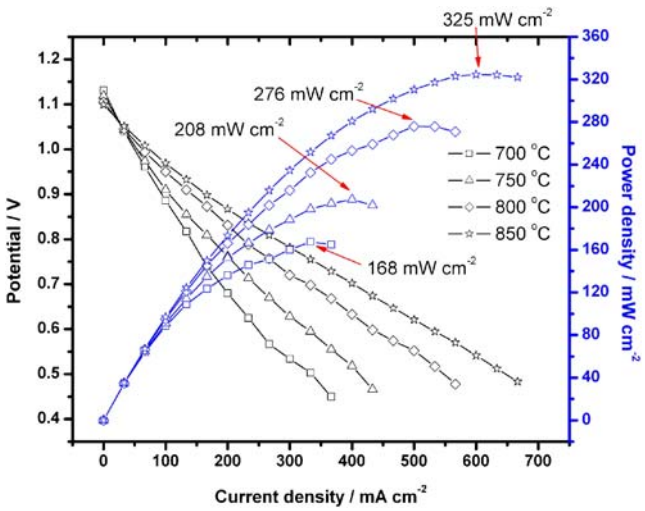

Fig. 8 The potential and power density versus the current density of the tubular SOFC at different temperatures using humidified H_2 as fuel and O_2 as oxidant

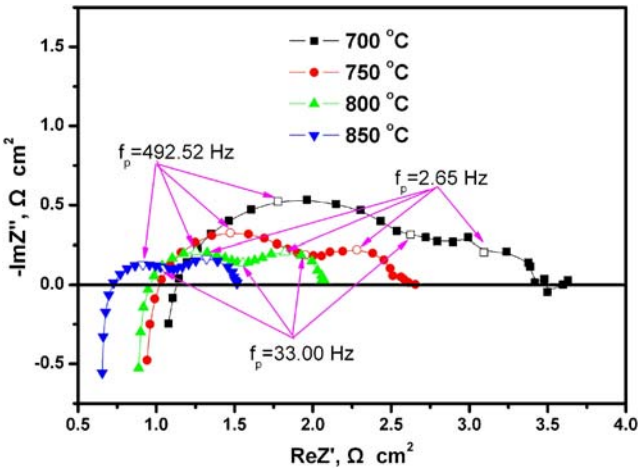

Fig. 9 AC impedance spectra for the anode-supported tubular SOFC under open circuit at different temperatures using humidified H_2 as fuel and O_2 as oxidant

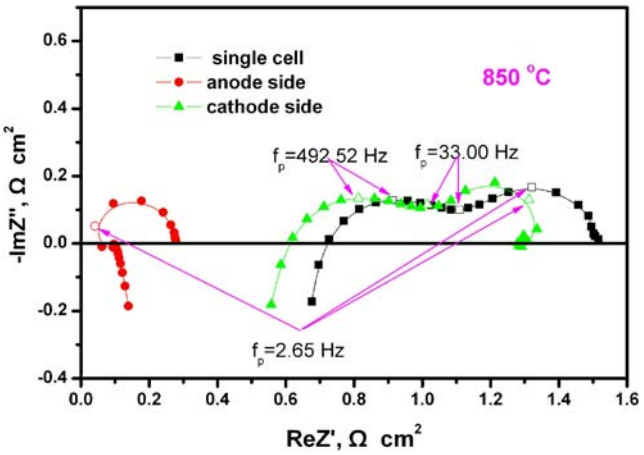

Fig. 11 AC impedance spectra for the single cell, the anode side, and the cathode side under open circuit at 850 °C using humidified H_2 as fuel and O_2 as oxidant

current densities of 0, 66.7, and 133 mA cm^{-2}, respectively. This phenomenon was attributed to the current, as the larger current density increased the electrochemical activity in the electrode.

Figure 11 shows the AC impedance spectra for the single cell, the anode side, and the cathode side under open circuit at 850 °C. The ohmic resistances and polarization resistances of the single cell, the anode side and the cathode side were, respectively, 0.72 and 0.80, 0.10 and 0.18, 0.62, and 0.68 Ω cm^2. The anode side resistance consists of the ohmic resistances of the electrolyte, the anode, the interface of the anode/electrolyte (R_Ω), and the polarization resistance (R_E) of the anode. The cathode side resistance consists of the ohmic resistances of the electrolyte, the cathode, the interface of the cathode/electrolyte (R_Ω), and the polarization resistance (R_E) of the cathode. The electrical conductivity of the ScSZ electrolyte was 0.178 S cm^{-1} at 850 °C [24], so the area specific resistance of the ScSZ electrolyte with a thickness of approx. 10 μm was approx. 5.6×10^{-3} Ω cm^2, which was very small compared to the total resistance. So, the ohmic resistance of the cathode/electrolyte interface and the polarization resistance of the cathode dominated the total resistance of the cell.

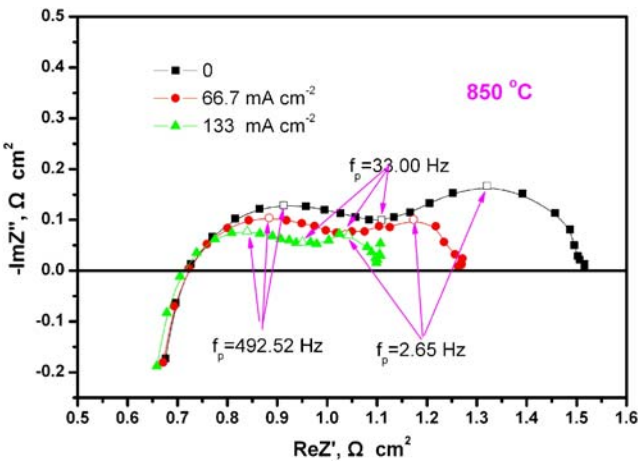

Fig. 10 AC impedance spectra for the anode-supported tubular SOFC under different current densities at 850 °C using humidified H_2 as fuel and O_2 as oxidant

Conclusions

An anode-supported tubular SOFC of 1.0 cm diameter has been successfully fabricated by the dip-coating method and tested at intermediate temperatures (under 850 °C). The cell consisted of a NiO-YSZ anode support tube, a NiO-ScSZ anode functional layer, a ScSZ electrolyte film, a LSM-ScSZ cathode functional layer, and a LSM cathode current collecting layer. The single tubular cell, which was 10.8 cm in length (cathode length=4.8 cm) generated 325, 276, 208, and 168 mW cm^{-2} at 850, 800, 750, and 700 °C, respectively, with humidified hydrogen and oxygen used as the working gases. The AC impedance spectra for the cell indicated that the most significant problem was on the cathode side; in particular, the ohmic resistance of the cathode/electrolyte interface was large. Further work is required to optimize the microstructure of the fuel cell, for example, to improve the method used for sintering in order to decrease the ohmic resistance of the cathode/electrolyte interface, with a view to achieving a better performance of the anode-supported tubular cell. Fabrication of new tubular

SOFCs in order to enhance the performance is currently being undertaken.

References

1. Du Y, Sammes NM (2004) J Power Sources 136:66. doi:10.1016/j.jpowsour.2004.05.028
2. Dong D, Gao J, Liu X, Meng G (2007) J Power Sources 165:217. doi:10.1016/j.jpowsour.2006.10.098
3. Setoguchi T, Sawano M, Eguchi K, Arai H (1990) Solid State Ion 40–41:502. doi:10.1016/0167-2738(90)90390-D
4. Schoonman J, Dekker JP, Broers JW, Kiwiet NJ (1991) Solid State Ion 46:299. doi:10.1016/0167-2738(91)90229-5
5. van Dieten VEJ, Schoonman J (1992) Solid State Ionics 57:141. doi:10.1016/0167-2738(92)90076-2
6. Chen CC, Nasrallah MM, Anderson HU (1994) Solid State Ion 70–71:101. doi:10.1016/0167-2738(94)90293-3
7. Hibino T, Hashimoto A, Asano K, Yano M, Suzuki M, Sano M (2002) Electrochem Solid-State Lett 5:A242. doi:10.1149/1.1508551
8. Shao Z, Haile SM (2004) Nature 431:170. doi:10.1038/nature02863
9. Steele BCH (1999) Nature 400:619. doi:10.1038/23144
10. Tsai T, Barnett SA (1995) J Electrochem Soc 142:3084–3087. doi:10.1149/1.2048692
11. de Souza S, Visco SJ, De Jonghe LC (1997) J Electrochem Soc 144:L35. doi:10.1149/1.1837484
12. Muccillo P, Muccillo ENS, Fonseca FC, Franca YV, Porfirio TC, de Florio DZ, Berton MAC, Garcia CM (2006) J Power Sources 156:455. doi:10.1016/j.jpowsour.2005.06.021
13. Sammes NM, Du Y, Bove R (2005) J Power Sources 145:428. doi:10.1016/j.jpowsour.2005.01.079
14. Kendall K, Palin M (1998) J Power Sources 71:268. doi:10.1016/S0378-7753(97)02761-4
15. Yashiro K, Yamada N, Kawada T, Hong J, Kaimai A, Nigara Y, Mizusaki J (2002) Electrochemistry 70(12):958
16. Kim JH, Songa RH, Song KS, Hyun SH (2003) J Power Sources 122:138. doi:10.1016/S0378-7753(03)00431-2
17. Suzuki T, Yamaguchi T, Fujishiro Y, Awano M (2006) J Power Sources 160:73. doi:10.1016/j.jpowsour.2006.01.037
18. Funahashi Y, Shimamori T, Suzuki T (2007) J Power Sources 163:731. doi:10.1016/j.jpowsour.2006.10.002
19. Li CJ, Li CX, Xing YZ, Gao M, Yang GJ (2006) Solid State Ion 177:2065. doi:10.1016/j.ssi.2006.03.004
20. Li CJ, Li CX, Ning XJ (2004) Vacuum 73:699. doi:10.1016/j.vacuum.2003.12.096
21. Li S, Wang S, Nie H, Wen T (2006) J Solid State Electrochem 11:59. doi:10.1007/s10008-005-0067-x
22. Kim JH, Song RH, Song KS, Hyun SH (2003) J Power Sources 122:138. doi:10.1016/S0378-7753(03)00431-2
23. Haanappel VAC, Mertens J, Rutenbeck D, Tropartz C, Herzhof W, Sebold D, Tietz F (2005) J Power Sources 141:216. doi:10.1016/j.jpowsour.2004.09.016
24. Yamamoto O (2000) Electrochim Acta 45:2423. doi:10.1016/S0013-4686(00)00330-3